

Controlling amyloid growth in multiple dimensions

JIJUN DONG, KUN LU, AMI LAKDAWALA*, ANIL K. MEHTA, & DAVID G. LYNN

Center for the Analysis of Supramolecular Self-assemblies, Departments of Chemistry and Biology, Emory University, Atlanta, GA 30322, USA

Keywords: Amyloid fibrils, nanotube, ribbon, β -sheet, lamination, structure

Abbreviations: AD = Alzheimer's disease; A β PP = Amyloid precursor protein; A β = Amyloid β peptide; AFM = atomic force microscopy; TM = transmembrane domain; CD = circular dichroism; FT-IR = Fourier transform infrared spectroscopy; MD = molecular dynamics; MRE = mean residue ellipticity; NMR = nuclear magnetic resonance; SSNMR = solid-state nuclear magnetic resonance; SANS/SAXS = small angle neutron scattering/small angle X-ray scattering; TEM = transmission electron microscopy; XAS = X-ray absorption spectroscopy

Abstract

The great progress made in defining the structure of protein and peptide amyloid assemblies, particularly the arrangement of peptides in β -sheets, is counterbalanced by the still poor understanding of the higher organization of β -sheets within the fibril and overall fibril/fibril associations. The assembly pathway and basis of amyloid toxicity may well depend on these higher-order structural features. For example, significant evidence points to association between sheets as the rate limiting step in fibril assembly, and a critical metal binding site has now been identified that involves residues from different individual sheets. Here we review experiments that are identifying some of the issues associated with sheet-sheet association by investigating simple model peptides derived from the central core of the A β peptide implicated in Alzheimer's disease. These peptides transit between fibril/ribbon/nanotube morphologies in response to assembly conditions, laying the foundation for understanding the folding landscape for these higher order assemblies, revealing potential targets for therapeutic intervention, and opening strategies for the design of highly ordered peptide self-assembled microscale morphologies.

Alzheimer's disease and Amyloid β peptide

More than 20 widely different maladies, including Alzheimer's, Parkinson's, Huntington's and human prion diseases, are recognized as protein conformational disorders [1,2]. Each disease is correlated with a specific protein conformational rearrangement that promotes self-aggregation and the loss of cellular function [3,4]. Although the proteins identified in these diseases have very different primary sequence and biochemical function, the aggregated forms, termed 'amyloid', share many common characteristics. These features include pleated β -sheet rich, non-branching fibrils with average diameters of 7–10 nm, association with specific histochemical dyes such as Congo Red [5], in this case, showing a unique 'apple-green' birefringence under crossed-polarized illumination, and resistance to proteolysis and chemical solubilization.

Alzheimer's disease (AD), the most widely recognized of the conformational disorders, is a late-onset, progressive and devastating neurodegenerative

disease characterized in individuals by loss of memory, task performance, and recognition of people and objects. AD now represents a major disease among aging populations, affecting approximately 25 million people worldwide, and the associated health care costs are growing rapidly [6]. The characteristic pathology of AD patients is associated with extracellular neuritic plaque deposits as well as intracellular neurofibrillary tangles in brain tissues. The amyloid plaques are composed of aggregates of the β -amyloid peptide (A β), a 39–43-amino acid proteolytic fragment of a larger transmembrane protein termed amyloid precursor protein (A β PP) (Figure 1).

Full length A β consists of 28 amino acids of the extracellular domain at the N-terminus and 11–14 amino acids of the adjacent transmembrane (TM) domain of A β PP. The A β sequence can be commonly defined with four distinct domains: a hydrophilic N-terminus, a central hydrophobic region (residues 17–21), a small central hydrophilic region (residues 22–28), and a long and very hydrophobic C-terminus (residues 29–43). Besides full length A β

Correspondence: David G. Lynn, Center for the Analysis of Supramolecular Self-assemblies, Departments of Chemistry and Biology, Emory University, 1515 Dickey Dr. NE, Atlanta, GA 30322, USA. Tel: +1 404 727 9348. Fax: +1 404 727 6586. E-mail: david.lynn@emory.edu

*Present address: GlaxoSmithKline, 709 Swedeland Road, UW2941, PO Box 1539, King of Prussia, PA 19406, USA.



Figure 1. The amino acid sequence of β -amyloid peptide ($A\beta$) and its location within Amyloid Precursor Protein ($A\beta$ PP). The transmembrane (TM) region of $A\beta$ PP is defined between two vertical thin lines.

peptide, many different lengths of $A\beta$ have been identified *in vivo* including N-terminus truncations at residues 1, 2, 4, 8, 11, and 17 [7,8]. The tendency of different fragments to associate with the fibrillar state, or putative disease state, is significantly different. $A\beta(1-40)$ is the most prevalent $A\beta$ sequence found in AD, consisting of about 90% of all $A\beta$, but it appears to be a more minor component in $A\beta$ deposits and to contribute only to later phases of the disease pathology [9]. The major component in these deposits is $A\beta(1-42)$ [10-12].

Although the pathological role of $A\beta$ is unclear, this soluble peptide is present in all individuals at picomolar concentrations [13,14], and the transition from soluble $A\beta$ to a non-native conformation capable of aggregation into fibrils appears intimately associated with disease progression [15]. Accordingly, efforts to understand the structural nature of amyloid fibrils and to determine the factors affecting or participating in self-assembly could be crucial to therapeutic intervention. Such understanding could also reveal fundamental principles regarding self-assemblies in other conformational diseases.

Structural characterization of amyloid fibrils *in vitro*

The characterization of $A\beta$ peptide congener self-assembly *in vitro* has revealed much about the structure and kinetics of amyloid formation. Many of these peptides produce fibrils which are morphologically, histochemically, immunologically, and spectroscopically indistinguishable from *ex vivo* fibrils. Even *in vitro* however, working with $A\beta$ remains challenging as the peptides have poor solubility and a tendency to precipitate amorphously. Consequently, high-resolution structural characterization of amyloid fibrils, by solution nuclear magnetic resonance (NMR) and/or X-ray crystallography, has been limited by the large molecular weight, insolubility, and para-crystallinity of the aggregated $A\beta$ peptides.

Amyloid fibril architecture has been characterized at low resolution by infra-red spectroscopy (IR), circular dichroism (CD), electron microscopy (EM), and X-ray fiber diffraction. These analyses established a cross- β pattern [16] composed of β -strands with the associated β -sheet hydrogen bonds oriented

parallel to fibril long axis. In particular, X-ray diffraction reflections at ~ 5 and ~ 10 Å have been interpreted as corresponding to the spacing between strands in the sheet and the mean distance between peptides in neighboring sheets, respectively (Figure 2C) [17-19]. Such cross- β patterns have been observed for amyloid fibrils formed by many other proteins, implying a common self-assembled architecture [20,21]. Largely based on IR measurements, the orientation of β strands within the β -sheet was interpreted early on as anti-parallel for a range of $A\beta$ peptides, including $A\beta(34-42)$ and $A\beta(X-43)$ where $X=1, 2, 4, 8, 9, 10, 12$ [22,23].

More recently, solid-state NMR (SSNMR) methods have defined the precise position of peptides within a sheet by accurate measurements of inter-strand backbone carbonyl-carbonyl and/or carbonyl-amide distances. The overall strategy, the first to give high resolution constraints between amyloid peptides [24,25], was developed on $A\beta(10-35)$. This peptide not only forms aggregate fibrils homologous to those of $A\beta(1-40)$ and $A\beta(1-42)$ (Figure 2C), but also retains important features of the $A\beta$ peptide such as an essential central hydrophobic segment (residues 17-21) and a portion of the C-terminus hydrophobic segment (residues 27-35) of $A\beta$ (Figures 2A and Figure 1). In addition, the first 10 residues at the N-terminus of $A\beta(1-40)$ are known to be disordered and susceptible to proteolytic cleavage [8,26,27], whereas residues 11-42 appear to maintain a more well-defined, uniform secondary structure [28]. Precise distance measurements from SSNMR at the backbone carbonyls of residues 12, 15-18, 20, 24-26, 29, 33, and 34 established that the entire $A\beta(10-35)$ peptide stacks in a parallel, in-register orientation throughout the length of the fibril (Figure 2B). The fiber is composed of six such parallel β -sheets as defined by small angle neutron scattering (Figure 2C) (see Ref. [29] for review). The parallel arrangement of the fibrils formed by full length $A\beta$ peptides was independently confirmed and further extended [30].

To date, however, very few structural constraints on the precise arrangement of the sheets within the fibril or the orientation between associating individual fibrils have been obtained. For example, the sheets could assemble in parallel or antiparallel

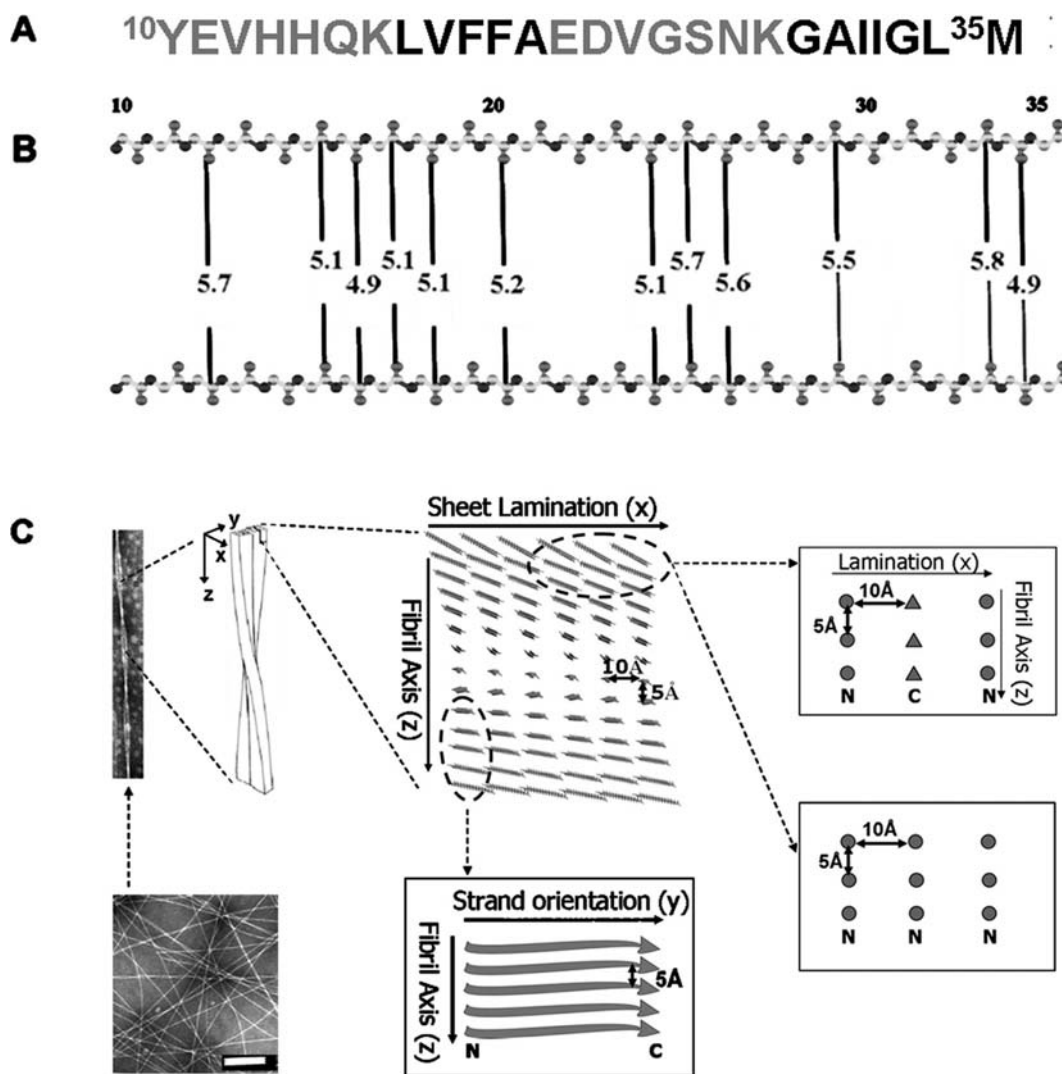


Figure 2. (A) Sequence of $A\beta(10-35)$. The sequence is color coded roughly based on the hydrophobicity of the amino acids and presented as alternative hydrophilic (grey) and hydrophobic (black) regions. (B) Experimental distances of inter-peptide ^{13}C -carbonyl contacts observed for $A\beta(10-35)$ by SSNMR. Inter peptide distances were measured at positions V12, Q15–V18, F20, V24–G26, G29, G33, and L34. Glycine residues and residues proximal to glycine exhibited larger distances and greater measurement error, $\pm 0.4 \text{ \AA}$, attributable to flexibility or disorder. Light grey, carbon; dark grey, oxygen; black, nitrogen. (C) Structural model of the $A\beta(10-35)$ fibril. (Left) Typical TEM image of amyloid fibrils (scale bar 200 nm) and a twisted pair, as well as a cartoon representation of one repeat of such fibrils. (Center) Schematic demonstration of the microstructure within one fibril. In this structural model, amyloid fibril is defined by growth along three orthogonal planes, β -strand association along z , sheet-sheet lamination in x , and layering in y . Single line represents the backbone of one $A\beta(10-35)$ molecule; the arrow head indicates the C-terminus of the $A\beta(10-35)$ peptide. Parallel in-register β -strands (lower center) orient perpendicular to and twist along the fibril long axis (z -axis) with 5 \AA spacing (upper center), while six such sheets laminate together along the x -axis with 10 \AA spacing (upper center). (Right) Relative orientations of sheets along the lamination dimension, parallel (lower right) or anti-parallel (upper right). Viewed down the peptide backbone, circles represent peptide N-termini and triangles represent C-termini.

relative orientations as shown in Figure 2C. As the mean backbone distances between laminates appear to be $\sim 10 \text{ \AA}$, they are out of the range for direct carbonyl–carbonyl and/or carbonyl–amide backbone distance measurement by SSNMR. Moreover, sheet packing appears to be driven by different forces, the hydrophobic and electrostatic compatibility of the side chains rather than backbone hydrogen bonding, and the driving forces defining sheet lamination are expected to be less specific and weaker. Here we review progress made in

understanding the determinants governing sheet lamination and the relationships between β -sheet growth, β -sheet lamination, and fibril stacking.

Simulations of the structural model of $A\beta(10-35)$ fibrils

In the structural model for the $A\beta(10-35)$ fibril, the parallel in-register arrangement of the β -strands is well defined. However, such long extended parallel β -strands, in this case 26 amino acids, are

unprecedented in globular proteins. Searches of the Protein Data Bank for planar parallel β -sheets conformations suggested that long idealized β -strands are energetically prohibitive and that typical strand lengths normally stretch only across five to six residues [31,32]. To evaluate the energetic consequences of the $A\beta(10-35)$ structural model and explore the interplay between two distinct directions for fibril assembly, β -sheet growth and β -sheet stacking (β -sheet lamination), Lakdawala et al. performed molecular dynamic simulations (MD) on a 6×6 block, six parallel β -strands in six parallel β -sheets, of the fully hydrated $A\beta(10-35)$ fibril [31,32]. Indeed, a striking characteristic of the simulation was that at any given time only 20–25% of the possible backbone hydrogen bonds, defined as a CO–HN distance of 1.8–2.3 Å, are present (Figure 3). These hydrogen bonds appear in short blocks, where regions with more than a few hydrogen bonds appearing consecutively along the backbone of a single β -strand are rare. A significant number of backbone amides, those not forming traditional backbone hydrogen bonds, twist out-of-plane, ranging roughly 30–45°, consistently suggesting that strand energies limit the number of residues in sequential hydrogen bond registry [31,32].

More interestingly, the simulations suggested that the total number of H-bonds predicted within the fibril could remain constant even though their positions change over time. Statistically significant anti-correlated motions appear across adjacent sheets [32]. Figure 3 compares two adjacent sheets at the same time point; regions of larger deformity in the left half (*circled in black*) are accounted for by tight hydrogen bonded networks in the right; and *vice versa*. Such compensation throughout the fibril may contribute significantly to global stability, allowing for greater local deformations and overall fibril plasticity.

In contrast, the flexible hydrogen bonding network and the motions accessible between different sheets could well limit the total number of sheets that pack to define the fibril depth. Lu et al. [33] reasoned that

interactions between short peptide segments may well give better defined individual sheets with more restricted and ordered hydrogen bonded networks, and correspondingly increase the degree of lamination within the fibril. Indeed, previous studies have shown that fibrils formed by the longer $A\beta(1-40)$ may contain two to four laminates [28,34], while those by the shorter $A\beta(18-28)$ peptides contain as many as 24 laminates [19]. Most noticeably, $A\beta(16-22)$, the central fragment of $A\beta$ with only seven residues, is capable of self-assembly into novel nanotubes composed of as many as 130 laminates (Figure 4) [33].

Exploring β -sheet lamination in $A\beta(16-22)$

To physically explore the dynamic correlations between β -sheet growth and β -sheet stacking (β -sheet lamination), indicated by the MD simulation of $A\beta(10-35)$, Lu et al. further characterized the seven-residue peptide segment from $A\beta$, $A\beta(16-22)$ [33]. $A\beta(16-22)$ contains one of the most important hydrophobic regions of the $A\beta$ peptide [23,35–38]. Proline scanning through this region prevented assembly of the full length peptide [38], and inhibitors developed for full length amyloid fibril assembly, QKLVFF, KLVFF and LVFFA, simple peptides that are in clinical trials as potential drugs to treat Alzheimer's disease [39,40], contain this hydrophobic region [37,41]. $A\beta(16-22)$ itself was found to assemble into fibrils under physiological conditions [42]. X-Ray powder diffraction and optical birefringence confirmed the amyloid nature of the $A\beta(16-22)$ fibrils and a series of solid-state NMR measurements determined an antiparallel organization within the β -sheets [42]. This antiparallel organization has also been observed by simulations [43–45], and the electrostatic interaction between Glu and Lys was viewed as critical in stabilizing the strand orientation.

Reinvestigating these assemblies revealed that $A\beta(16-22)$ forms a range of morphologies at neutral

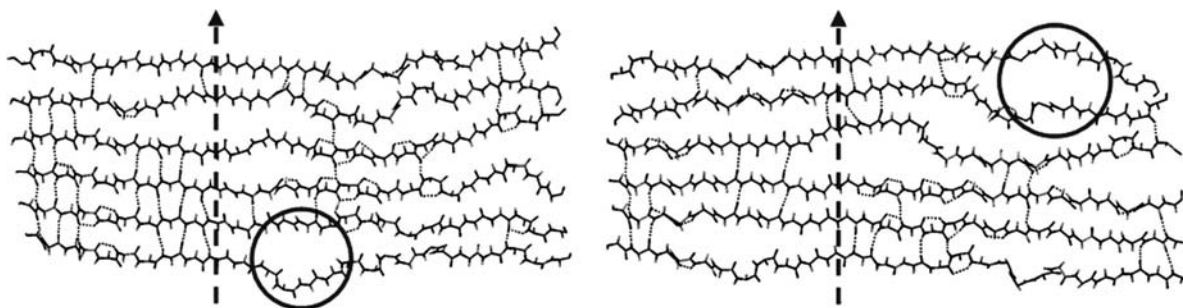


Figure 3. Comparison of adjacent laminate β -sheets in $A\beta(10-35)$ fibrils after 65 ps of MD at 100 K. Both side chains and water molecules have been removed for clarity. Black dashed lines represent H-bonds. The arrows indicate the direction of fibril z -axis. Major deformities (*highlighted in the circles*) in the sheet on the left are compensated for in the sheet on the right through hydrogen bonding networks, and *vice versa*.

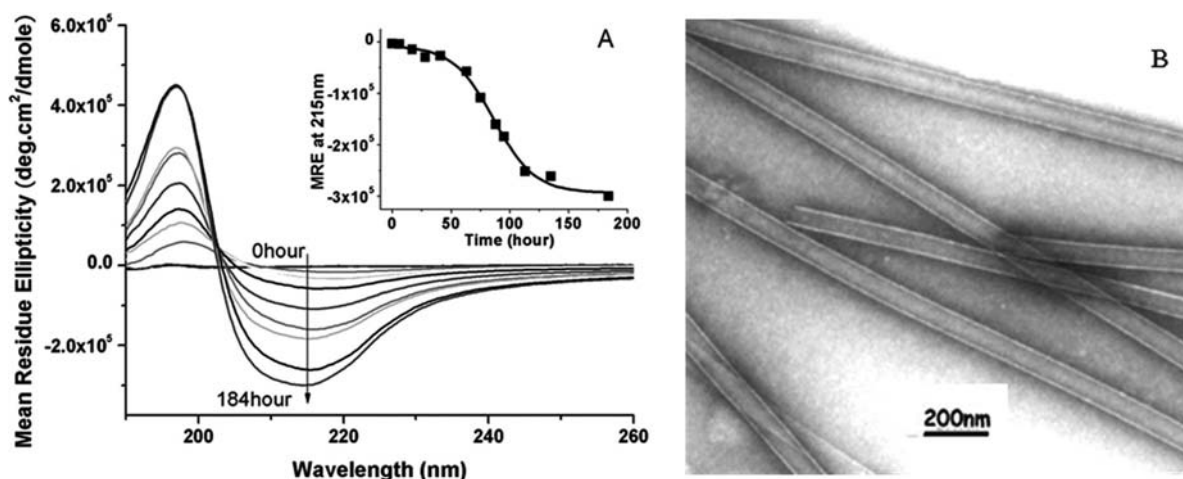


Figure 4. (A) Time-dependent CD spectra of $A\beta(16-22)$. Significant β -sheet signal develops in solution during incubation. The inset plots the mean residue ellipticity at 215 nm as a function of time for 1.3 mM $A\beta(16-22)$ dissolved in 40% acetonitrile/water with 0.1% TFA (pH 2). The line in the inset is a sigmoidal fit to the data, consistent with a nucleation-dependent growth. The time dependence can vary with very minor changes in assembly conditions [33]. (B) TEM micrographs of $A\beta(16-22)$ ~80-nm wide homogeneous assemblies after 2 weeks. Sharp white edges are suggestive of hollow tubular structures.

pH. Under acidic conditions, however, $A\beta(16-22)$ self-associates into homogeneous tubular structures whose morphology has now been characterized and confirmed by CD, SANS/SAXS, AFM and TEM studies (Figure 4). At pH 2, the glutamate side-chain at the C-terminus is expected to be protonated, leaving a single positive charge on the N-terminal lysine side chain in each peptide. The single positive charge provides an amphiphilicity that may be critical to fibril formation [33]. CD reveals a conformational conversion from random coil into β -sheet with an absolute mean residue ellipticity at 215 nm that is several-fold greater than seen for typical globular proteins or amyloid fibrils (Figure 4A). Since this simple $A\beta$ peptide has random coil conformation before assembly and shows no CD signal at 215 nm, the development of the ellipticity at 215 nm is a direct reflection of the amount of monomers that adopt β -sheet structure upon assembly. Thus, the sigmoidal time dependence of the ellipticity at 215 nm is consistent with a nucleation-dependent growth (Figure 4A, inset).

Further TEM analyses of the final assemblies showed structures maintaining a highly homogeneous width of 80 ± 5 nm (Figure 4b) and a poly-disperse contour length from 10 and several hundred microns, significantly larger than typical amyloid fibrils. Sharp white edges appear in the negative uranyl acetate stained samples, consistent with hollow structures flattened by dehydration. Helical ribbon intermediates were observed by both TEM and AFM, with a width of ~ 130 nm and a height of ~ 4 nm at the lowest point and ~ 8 nm at the highest point. These ribbons were able to access a left or right handed helical pitch and appear to fuse into nanotube structures [33]. Bessel oscillations in

$I(Q)$, characteristic of a hollow cylindrical form factor, were observed both in SANS and SAXS experiments on these soluble self-assemblies [46], and the data are well described by a mono-disperse system of hollow cylinders with an outer radius of 26 nm and a wall thickness of 4 nm. The 4-nm thick tube walls, consistent with the AFM analyses, are roughly twice the length of the $A\beta(16-22)$ β -strand peptide.

Therefore, direct extensions of the structural model for $A\beta(10-35)$ (Figure 2C) could readily explain the tubular morphology accessed by $A\beta(16-22)$ (Figure 5). As in the fibrils, the hydrogen-bonding of the β -sheet would be parallel to the long axis of the ribbons. Consistent with the observation of twisted amyloid fibril dimers [29] and nanotubes with wall thickness of twice the peptide length that give the two leaflets of a peptide bilayer [33], the ribbon would arise by merely extending β -sheet lamination growth. A related peptide bilayer has also been proposed by Zhang et al. for nanotubes formed from surfactant-like peptides containing a hydrophilic head group of charged aspartic acids and a lipophilic tail made of leucine, alanine or valine [46]. This morphology for the $A\beta(16-22)$ ribbons and nanotubes are also similar to those formed by several other amphiphiles including lipids [47,48], bile acids [49], phenyl glucosides [50], diacetylenic aldonamides [51] and double chain glutamate derivatives [52], suggesting the bilayer morphology as readily accessible to a wide variety of different structural entities.

As shown in Figure 5C, the width of the intermediate peptide ribbon is defined by the number of β -sheet laminates which maintain a 10-Å spacing between the individual sheets. Correcting for the overestimate of the widths by AFM, the initial bilayer

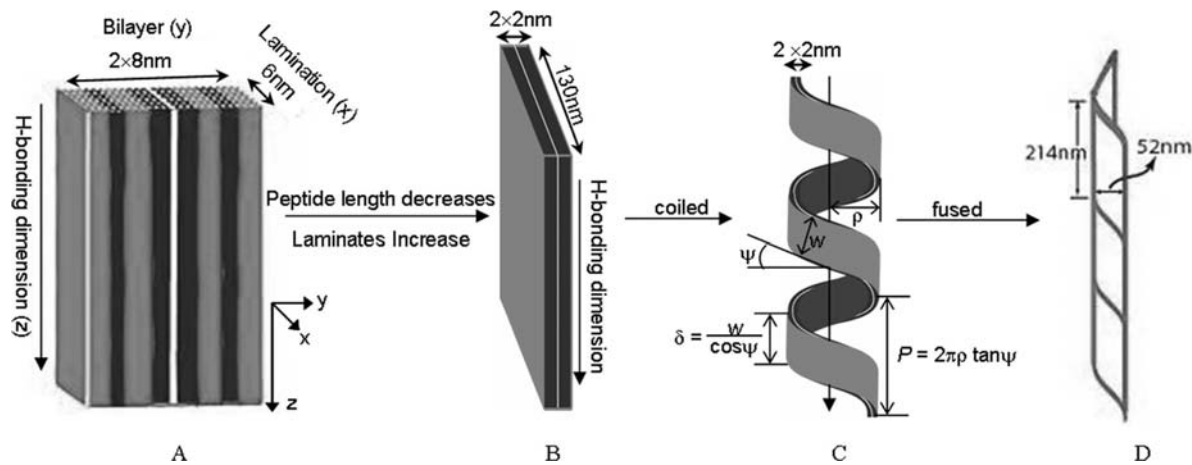


Figure 5. Model for self-assembly of Aβ(16–22) peptide nanotubes. Grey stands for the sequence region with dominant hydrophilic amino acids and black for sequence region with dominant hydrophobic amino acids. The white line represents the bilayer interface. (A) A bilayer model for Aβ(10–35) fibril. β-sheets with backbone H-bonds oriented along the long axis (z-axis) are pointed to each other, end to end, to form a peptide bilayer. The length of a 25 residue β-strand peptide is ~8 nm long. Lamination of six β-sheets is perpendicular to the long axis, defining the width of the bilayer. (B) After shortening the peptide length from 8 to 2 nm with Aβ(16–22), the lamination increases from 6 to 130 nm. (C) Laminated β-sheet bilayer coils up to form a helical ribbon. The geometry of the helical ribbon is described with the following parameters: ρ, radius; ω, pitch angle; P, pitch; w, width; δ, width along the z-axis. (D) Helical ribbon fuses into tubular structure with an outer diameter of 52 nm and an outer helical pitch of 214 nm.

ribbon of Aβ(16–22) would be composed of ~130 laminates [33], whereas the simple bilayer proposed for the Aβ(10–35) duplex fibril has only six laminates. Therefore, the degree of lamination has been dramatically extended merely by shortening the peptide length to seven residues. In order for the ribbon to twist so that the ends meet, yet maintain the same number of laminates, the outer leaflet of the bilayer requires a periodicity of 214 nm and the inner of 383 nm [33,49] (also see Figure 5 for the calculation). This pitch requires a 0.42° and 0.23° offset between adjacent outer and inner Aβ(16–22) strands, respectively, within a β-sheet [33]. In contrast, the offset for each Aβ(10–35) strand in the fibril (Figure 2C) requires a 1.6° offset [25].

Metal ion induced β-sheet lamination

As subtle changes in assembly conditions provide easily scored morphological alterations in assembly architecture, Aβ(16–22) becomes a valuable system for the evaluation of lamination energetics. Changes in protonation are difficult to evaluate structurally, and metal ion association with basic sites were viewed as providing rich spectroscopic handles. Increasingly, the role of Zn²⁺ and other metal ions in amyloid aggregation, neurotoxicity, and Alzheimer's disease (AD) are being highlighted [53–55]. Zn²⁺ concentrations above 300 nM rapidly precipitate Aβ(1–40) [54]. It has been shown that Aβ(1–40) binds multiple Zn²⁺ ions and a high affinity nanomolar site has been reported [56–60]. Mutagenesis and pH dependence studies of Zn²⁺ induced Aβ aggregation have suggested that histidine-13 is crucial for Zn²⁺

binding [25,58–62]. Moreover, rat Aβ(1–40), with substitutions of R5 → G, Y10 → F and H13 → R, binds Zn²⁺ much more weakly [53,54]. The exact coordination environment and geometry of the Zn²⁺–Aβ complex, however, remains a critical and most important unresolved issue in AD. Zn²⁺ is unfortunately spectroscopically silent as metals go, contributing significantly to the lack of structural and chemical information currently available.

Morgan et al. explored the strong and specific metal binding to Aβ as both a structural and kinetic probe for Aβ self-assembly [61]. In a cross β-sheet model with parallel in-register arrangement of β-strands along the fibril axis as shown for Aβ(10–35) (Figure 2C), the side chains of His13 and His14 are directed to opposite β-sheet surfaces and spaced at 5-Å intervals along each face (Figure 6A). If the sheets are positioned parallel to one another, residues His13 and His14 from different sheets would also be positioned in close proximity (Figure 6B). Therefore, there are at least two potential binding sites (Figure 6A, B), and in the simple model peptides below, the question of metal association can be simplified to determining whether Zn²⁺ is binding along or between β-sheets.

Aβ(13–21), HHQKLVFFA, a peptide including both the core segment Aβ(17–21) known to be crucial for fibril formation [24,25,33,63], and the putative metal binding HH dyad, was further explored for its ability to coordinate Zn²⁺. To isolate His13/14 as the sole binding elements, Dong et al. prepared the K16A peptide, Aβ(13–21)K16A [64]. Aβ(13–21)K16A develops β-sheet secondary structure and assembles into typical amyloid fibrils

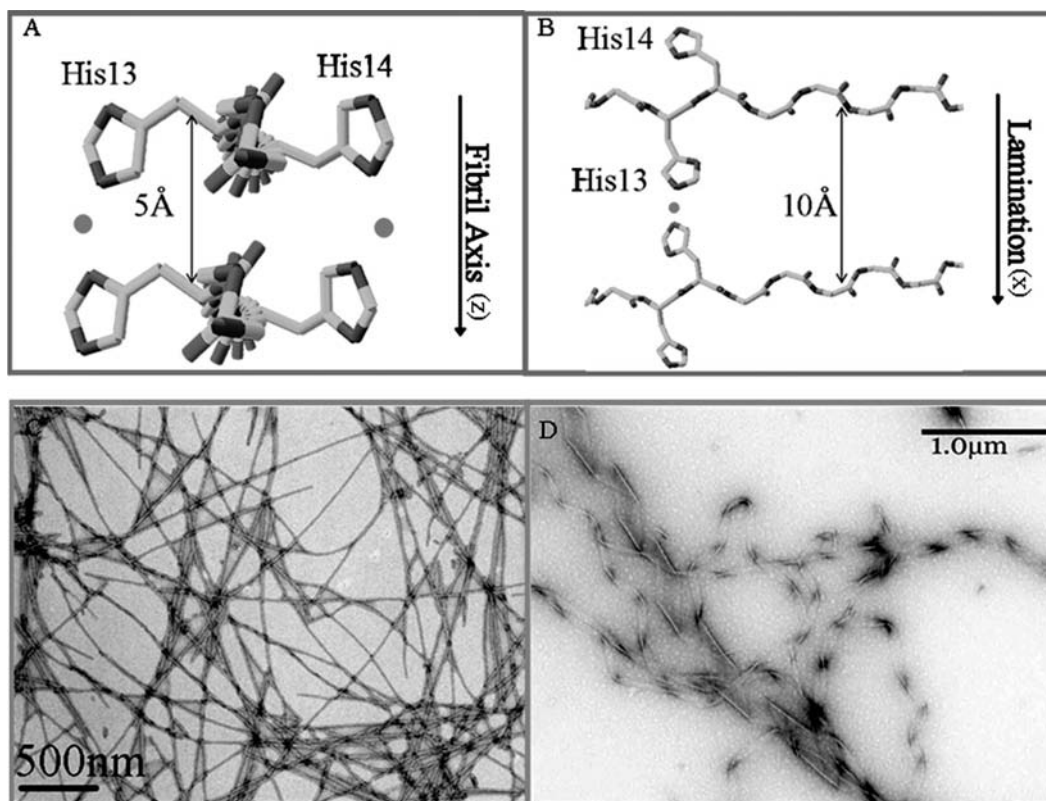


Figure 6. (A) Potential Zn^{2+} -binding sites (indicated with the dark grey spheres) formed between two β strands within a sheet, as viewed along the peptide backbone and perpendicular to the axis of fibril propagation. (B) Potential Zn^{2+} -binding site formed between two strands of adjacent sheets, as viewed down the axis of fibril propagation. In both A and B, only the backbone and His side chain atoms are shown. Light grey, carbon; black, oxygen and nitrogen. Dark grey sphere, metal ion. (C) TEM image of $\text{A}\beta(13-21)\text{K16A}$ amyloid fibrils. (D) TEM images of twisted ribbons with variable width formed from $\text{A}\beta(13-21)\text{K16A}$ in the presence of one equivalent of Zn^{2+} .

(Figure 6C) [64]. Preliminary solid-state NMR and isotope editing FTIR results imply a parallel in-register β -sheet orientation of the peptides in the assemblies [64]. However, the presence of Zn^{2+} dramatically alters both self-assembly kinetics and morphology. The nucleation time is virtually eliminated with 1 equivalent of Zn^{2+} , and this rapid assembly is accompanied by the formation of helical 5 ± 0.5 nm thick ribbons with widths of 30–50 nm. Wider 100–150 nm ribbons with variable twists form with longer incubation times (Figure 6D). Some of the ribbons appear to coil and fuse to form tubular structures with widths of 200–300 nm [64]. The coordination environment of Zn^{2+} in the assemblies was resolved by X-ray absorption spectroscopy (XAS); fitting of the XAS spectra indicated that Zn^{2+} is indeed associated with two His residues in the assembled Zn^{2+} - $\text{A}\beta$ complexes [64].

More strikingly, when the Zn^{2+} to peptide ratio is dropped to 0.2 from 1.0, Zn^{2+} induces typical amyloid fibrils, similar to $\text{A}\beta(10-21)$ [61], and yet the coordination to two His residues is retained [64]. Although the identity of the other ligands that bind Zn^{2+} in $\text{A}\beta(13-21)\text{K16A}$ assemblies has not been fully defined, the XAS data reveals that Zn^{2+} chelates two His residues in both amyloid fibrils and twisted

ribbons/nanotubes, suggesting the existence of distinct His- Zn^{2+} -His coordination modes. Further studies imply that these distinct modes are defined by the relative position of the His residues – along a single β -sheet surface versus that between two adjacent sheets (Figure 6A, B), and the site accessibility is controlled by the assembly conditions [64]. In this model, Zn^{2+} chelation between β -sheets significantly stabilizes β -sheet lamination, giving rise to significant lamination growth, thereby altering the morphology from fibers to twisted ribbons. The accessibility of these specific metal sites in longer $\text{A}\beta$ peptides and/or in disease states can now be determined.

Amyloid diseases

Amyloid assemblies are presented here as stacks of β -sheet peptides whose morphology is defined by growth along three orthogonal planes, β -sheet association along z , sheet-sheet lamination in x , and layering in y (Figure 2C and Figure 5). Of these growth planes, peptide backbone H-bonding energetically dominates, defining the long z -axis of amyloid fibrils. Growth along the x and y directions are regulated by the specific peptide sequence and the conditions for assembly, and it is these planes that

define the fibril/ribbon morphology. It is only now that approaches which modulate the relative growth rate/stability along the different planes have emerged, enabling assembly of novel twisted helical ribbons and nanotubes from simple $A\beta$ segments. These initial glimpses into sheet lamination and layering of amyloid fibrils are structurally significant.

A hierarchal model has been developed to explain and predict different assembly morphologies, such as twisted fibrils, ribbons, and flat sheets/tapes [63]. This model predicts that the formation of twisted β -sheets results from the chirality of the peptide structural units, and that a maximal number of sheets will assemble when the energies of sheet-sheet attraction approximate the elastic costs associated with untwisting of individual β -sheets [63]. Based on this proposal, infinite stacks of sheets are accessible if sheet-sheet interactions are sufficiently strong and/or if the peptide monomers remain planar and untwisted. Indeed, shortening the peptide length and/or coordinating metal ions between sheets dramatically expands sheet-sheet lamination. For $A\beta(16-22)$, the short peptide could well access a more planar β -sheet and still maintain a fully hydrogen bonded network along the fibril long axis. Moreover, hydrophobic packing of the phenylalanine dyads, Phe 19/20, may be sufficient to increase the relative growth of the laminates, and a simple FF dipeptide has been reported to self-assemble [65]. Initial SSNMR evidence suggests that a one-residue shift in the peptide registry in the sheets of $A\beta(16-22)$ alters the relative position of the Phe dyad. (unpublished data) The resulting enhanced packing of the side-chains stabilizes and/or accelerates sheet-sheet association to give nanotubes, while the in-register arrangement gives fibrils. The study of these simple peptides will certainly continue to provide an experimental test bed for the predictions of the model, and an extension of this approach may well provide an understanding of the helical pitch necessary for homogeneous nanotube assembly.

Given the complex matrix of risk factors associated with amyloid diseases [66], it may well be the *context of amyloid assembly* that proves to be most central to disease etiology and severity. If all α -amino acid polymers have the potential to form amyloid [67], then only a very few of these amyloids must compromise cellular function and cause disease. Such disease states may well depend on the primary amino acid sequence of a particular peptide, but increasing evidence points toward the ability of different assemblies of the same peptide to result in toxicity. For example, different neurotoxicities have been observed for altered morphologies of $A\beta(1-40)$ [68]. Amyloid formation and self-propagation of yeast prion protein can give rise to diverse yeast phenotypes, and recent evidence suggests that such

phenotype diversity is a direct result of the specific assembly [69]. Here we specifically underscore the vital role of β -sheet lamination in the modulation of amyloid morphology. The degree to which β -sheet lamination, and therefore morphology, are altered by metal ion concentration, pH, changes in nucleation and propagation rates, and membrane surfaces and chaperon concentrations may well define etiology. Likewise, the altering amyloid morphology and clearance should be critical for $A\beta$ disease prevention and should serve as a model for therapeutic intervention in many other amyloid diseases. We therefore anticipate that studies on the regulation of the 3D growth of amyloid will provide critical new insights into strategies to direct assembly away from 'toxic amyloid assembly' toward materials that can be biologically cleared.

References

1. Carrell RW, Lomas DA. Conformational disease. *Lancet* 1997;350:134-138.
2. Kelly JW. The alternative conformations of amyloidogenic proteins and their multi-step assembly pathways. *Curr Opin Struct Biol* 1998;8:101-106.
3. Carrell RW, Gooptu B. Conformational changes and disease – serpins, prions and Alzheimer's. *Curr Opin Struct Biol* 1998; 8:799-809.
4. Ross CA, Poirier MA. Protein aggregation and neurodegenerative disease. *Nat Med* 2004;10:S10-17.
5. Nilsson MR. Techniques to study amyloid fibril formation in vitro. *Methods* 2004;34:151-160.
6. Koppel R. Alzheimer's disease: The costs to U.S. businesses in 2002. 2002. The Alzheimer's Association.
7. Nunan J, Small DH. Regulation of APP cleavage by α -, β - and γ -secretases. *FEBS Lett* 2000;483:6-10.
8. Saido TC, YamaoHarigaya W, Iwatsubo T, Kawashima S. Amino- and carboxyl-terminal heterogeneity of β -amyloid peptides deposited in human brain. *Neurosci Lett* 1996;215: 173-176.
9. Asami-Odaka A, Ishibashi Y, Kikuchi T, Kitada C, Suzuki N. Long amyloid β -protein secreted from wild-type human neuroblastoma IMR-32 cells. *Biochemistry* 1995;34:10272-10278.
10. Dovey HF, Suomensaaari-Chrysler S, Lieberburg I, Sinha S, Keim PS. Cells with a familial Alzheimer's disease mutation produce authentic β -peptide. *Neuroreport* 1993;4:1039-1042.
11. Naslund J, Schierhorn A, Hellman U, Lannfelt L, Roses AD, Tjernberg LO, Silberring J, Gandy SE, Winblad B, Greengard P. Relative abundance of Alzheimer $A\beta$ amyloid peptide variants in Alzheimer disease and normal aging. *Proc Natl Acad Sci USA* 1994;91:8378-8382.
12. Roher AE, Lowenson JD, Clarke S, Woods AS, Cotter RJ, Gowing E, Ball MJ. β -Amyloid-(1-42) is a major component of cerebrovascular amyloid deposits: implications for the pathology of Alzheimer disease. *Proc Natl Acad Sci USA* 1993;90:10836-10840.
13. Seubert P, Vigo-Pelfrey C, Esch F, Lee M, Dovey H, Davis D, Sinha S, Schlossmacher M, Whaley J, Swindlehurst C, et al. Isolation and quantification of soluble Alzheimer's β -peptide from biological fluids. *Nature* 1992;359:325-327.
14. Shoji M, Golde TE, Ghiso J, Cheung TT, Estus S, Shaffer LM, Cai XD, McKay DM, Tintner R, Frangione B, et al. Production of the Alzheimer amyloid β protein by normal proteolytic processing. *Science* 1992;258:126-129.

15. Hardy J. Has the amyloid cascade hypothesis for Alzheimer's disease been proved? *Curr Alzheimer Res* 2006;3:71–73.
16. Kirschner DA, Abraham C, Selkoe DJ. X-ray diffraction from intraneuronal paired helical filaments and extraneuronal amyloid fibers in Alzheimer disease indicates cross- β conformation. *Proc Natl Acad Sci USA* 1986;83:503–507.
17. Inouye H, Fraser PE, Kirschner DA. Structure of β -crystallite assemblies formed by Alzheimer β -amyloid protein analogues: analysis by X-ray diffraction. *Biophys J* 1993;64:502–519.
18. Inouye H, Kirschner DA. Refined fibril structures: the hydrophobic core in Alzheimer's amyloid β -protein and prion as revealed by X-ray diffraction. *Ciba Found Symp* 1996;199:22–35.
19. Kirschner DAI, Duffy LK, Sinclair A, Lind M, Selkoe DJ. Synthetic peptide homologous to β protein from Alzheimer Disease forms amyloid-like fibrils in vitro. *Proc Natl Acad Sci USA* 1987;84:6953.
20. Inouye H, Kirschner DA. X-ray diffraction analysis of scrapie prion: intermediate and folded structures in a peptide containing two putative alpha-helices. *J Mol Biol* 1997;268:375–389.
21. Nguyen JT, Inouye H, Baldwin MA, Fletterick RJ, Cohen FE, Prusiner SB, Kirschner DA. X-ray diffraction of scrapie prion rods and PrP peptides. *J Mol Biol* 1995;252:412–422.
22. Halverson K, Fraser PE, Kirschner DA, Lansbury PT Jr. Molecular determinants of amyloid deposition in Alzheimer's disease: conformational studies of synthetic β -protein fragments. *Biochemistry* 1990;29:2639–2644.
23. Hilbich C, Kisters-Woike B, Reed J, Masters CL, Beyreuther K. Aggregation and secondary structure of synthetic amyloid β A4 peptides of Alzheimer's disease. *J Mol Biol* 1991;218:149–163.
24. Benzinger TL, Gregory DM, Burkoth TS, Miller-Auer H, Lynn DG, Botto RE, Meredith SC. Two-dimensional structure of β -amyloid(10–35) fibrils. *Biochemistry* 2000;39:3491–3499.
25. Burkoth TS, Benzinger TLS, Urban V, Morgan DM, Gregory DM, Thiyagarajan P, Botto RE, Meredith SC, Lynn DG. Structure of the β -amyloid_(10–35) fibril. *J Am Chem Soc* 2000;122:7883–7889.
26. Roher AE, Lowenson JD, Clarke S, Wolkow C, Wang R, Cotter RJ, Reardon IM, Zurcherneckly HA, Heinrikson RL, Ball MJ, Greenberg BD. Structural alterations in the peptide backbone of β -amyloid core protein may account for its deposition and stability in Alzheimer's disease. *J Biol Chem* 1993;268:3072–3083.
27. Kheterpal I, Williams A, Murphy C, Bledsoe B, Wetzel R. Structural features of the A β amyloid fibril elucidated by limited proteolysis. *Biochemistry* 2001;40:11757–11767.
28. Petkova AT, Ishii Y, Balbach JJ, Antzutkin ON, Leapman RD, Delaglio F, Tycko R. Structural model for Alzheimer's β -amyloid fibrils based on experimental constraints from solid state NMR. *Proc Natl Acad Sci USA* 2002;99:16742–16747.
29. Lynn DG, Meredith SC. Model peptides and the physico-chemical approach to β -amyloids. *J Struct Biol* 2000;130:153–173.
30. Balbach JJ, Petkova AT, Oyler NA, Antzutkin ON, Gordon DJ, Meredith SC, Tycko R. Supramolecular structure in full-length Alzheimer's β -amyloid fibrils: evidence for a parallel β -sheet organization from solid-state nuclear magnetic resonance. *Biophys J* 2002;83:1205–1216.
31. Morgan DM, Lynn DG, Lakdawala AS, Snyder JP, Liotta DC. Amyloid structure: Models and theoretical considerations in fibrous aggregates. *J Chin Chem Soc-Taip* 2002;49:459–466.
32. Lakdawala AS, Morgan DM, Liotta DC, Lynn DG, Snyder JP. Dynamics and fluidity of amyloid fibrils: A model of fibrous protein aggregates. *J Am Chem Soc* 2002;124:15150–15151.
33. Lu K, Jacob J, Thiyagarajan P, Conticello VP, Lynn DG. Exploiting amyloid fibril lamination for nanotube self-assembly. *J Am Chem Soc* 2003;125:6391–6393.
34. Garzon-Rodriguez WS-B, Milton S, Glabe CG. Soluble amyloid A β -(1–40) exists as a stable dimer at low concentrations. *J Biol Chem* 1997;272:21037.
35. Fay DS, Fluet A, Johnson CJ, Link CD. In vivo aggregation of β -amyloid peptide variants. *J Neurochem* 1998;71:1616–1625.
36. Hilbich C, Kisters-Woike B, Reed J, Masters CL, Beyreuther K. Substitutions of hydrophobic amino acids reduce the amyloidogenicity of Alzheimer's disease β A4 peptides. *J Mol Biol* 1992;228:460–73.
37. Tjernberg LON, Lindqvist F, Johansson, J, Karlstrom AR, Thyberg, J, Terenius L, Nordstedt, C. Arrest of β -amyloid fibril formation by a pentapeptide ligand. *J Biol Chem* 1996;271:8545–8548.
38. Wood S, Wetzel R, Martin JD, Hurlle M. Prolines and amyloidogenicity in fragments of the Alzheimer's peptide. *Biochemistry* 1995;34:724–730.
39. Wolfe M. Therapeutic strategies for Alzheimer's disease. *Nat Rev Drug Discov* 2002;1:859.
40. Findeis M. Peptide inhibitors of β amyloid aggregation. *Curr Top Med Chem* 2002;2:417.
41. Findeis M, Musso GM, Arico-Muendel CC, Benjamin HW, Hundal AM, Lee JJ, Chin J, Kelley M, Wakefield J, Hayward NJ, Molineaux SM. Modified-peptide inhibitors of amyloid β -peptide polymerization. *Biochemistry* 1999;38:6791.
42. Balbach JJ, Antzutkin ON, Leapman RD, Rizzo NW, Dyda F, Reed J, Tycko R. Amyloid fibril formation by A β 16–22, a seven-residue fragment of the Alzheimer's β -amyloid peptide, and structural characterization by solid state NMR. *Biochemistry* 2000;39:13748–13759.
43. Ma B, Nussinov R. Stabilities and conformations of Alzheimer's β -amyloid peptide oligomers (A β 16–22, A β 16–35, and A β 10–35): Sequence effects. *Proc Natl Acad Sci USA* 2002;99:14126–14131.
44. Santini SM, Derreumaux P. In silico assembly of Alzheimer's A β 16–22 peptide into β -sheets. *J Am Chem Soc* 2004;126:11509–11516.
45. Santini S, Mousseau N, Derreumaux P. Pathway complexity of Alzheimer's β -amyloid A β 16–22 peptide assembly. *Structure* 2004;12:1245–1255.
46. Vauthey SS, Gong H, Watson, N, Zhang S. Molecular self-assembly of surfactant-like peptides to form nanotubes and nanovesicles. *Proc Natl Acad Sci USA* 2002;99:5355–5360.
47. Fuhrhop JHW. Fluid and solid fibers made of lipid molecular bilayers. *Chem Rev* 1993;93:1565.
48. Schnur JM. Lipid tubules: A paradigm for molecularly engineered structures. *Science* 1993;262:1669.
49. Chung DSB, Konikoff FM, Donovan JM. Elastic free energy of anisotropic helical ribbons as metastable intermediates in the crystallization of cholesterol. *Proc Natl Acad Sci USA* 1993;90:11341.
50. Jung JHJ, Yoshida K, Shimizu T. Self-assembling structures of long-chain phenyl glucoside influenced by the introduction of double bonds. *J Am Chem Soc* 2004;124:10674.
51. Frankel DAOB. Supramolecular assemblies of diacetylenic aldonamides. *J Am Chem Soc* 1991;113:7436.
52. Nakashima NA, Kunitake T. Optical microscopic study of helical superstructures of chiral bilayer membranes. *J Am Chem Soc* 1985;107:509.
53. Bush AI, Pettingell WH, Multhaup G, Paradis MD, Vonsattel JP, Gusella JF, Beyreuther K, Masters CL, Tanzi RE. Rapid induction of Alzheimer A β amyloid formation by zinc. *Science* 1994;265:1464–1467.
54. Bush AI, Pettingell WH, Paradis MD, Tanzi RE. Modulation of A β adhesiveness and secretase site cleavage by zinc. *J Biol Chem* 1994;269:12152–12158.

55. Bush AI. The metallobiology of Alzheimer's disease. *Trends Neurosci* 2003;26:207–214.
56. Atwood CS, Moir RD, Huang XD, Scarpa RC, Bacarra NME, Romano DM, Hartshorn MK, Tanzi RE, Bush AI. Dramatic aggregation of Alzheimer A β by Cu(II) is induced by conditions representing physiological acidosis. *J Biol Chem* 1998;273:12817–12826.
57. Curtain CC, Ali F, Volitakis I, Cherny RA, Norton RS, Beyreuther K, Barrow CJ, Masters CL, Bush AI, Barnham KJ. Alzheimer's disease amyloid- β binds copper and zinc to generate an allosterically ordered membrane-penetrating structure containing superoxide dismutase-like subunits. *J Biol Chem* 2001;276:20466–20473.
58. Liu ST, Howlett G, Barrow CJ. Histidine-13 is a crucial residue in the zinc ion-induced aggregation of the A β peptide of Alzheimer's disease. *Biochemistry* 1999;38:9373–9378.
59. Miura T, Suzuki K, Kohata N, Takeuchi H. Metal binding modes of Alzheimer's amyloid β -peptide in insoluble aggregates and soluble complexes. *Biochemistry* 2000;39:7024–7031.
60. Yang DS, McLaurin J, Qin K, Westaway D, Fraser PE. Examining the zinc binding site of the amyloid- β peptide. *Eur J Biochem* 2000;267:6692–6698.
61. Morgan DM, Dong J, Jacob J, Lu K, Apkarian RP, Thiyagarajan P, Lynn DG. Metal switch for amyloid formation: insight into the structure of the nucleus. *J Am Chem Soc* 2002;124:12644–12645.
62. Zirah S, Kozin SA, Mazur AK, Blond A, Cheminant M, Segalas-Milazzo I, Debey P, Rebuffat S. Structural changes of region 1–16 of the Alzheimer disease amyloid beta-peptide upon zinc binding and in vitro aging. *J Biol Chem* 2006;281:2151–2161.
63. Aggeli A, Nyrkova IA, Bell M, Harding R, Carrick L, McLeish TC, Semenov AN, Boden N. Hierarchical self-assembly of chiral rod-like molecules as a model for peptide β -sheet tapes, ribbons, fibrils, and fibers. *Proc Natl Acad Sci USA* 2001;98:11857–11862.
64. Dong JJ, Shokes JE, Scott RA, Lynn DG. Modulating amyloid self-assembly and fibril morphology with Zn(II). *J Am Chem Soc* 2006;128:3540–3542.
65. Gazit E. A possible role for pi-stacking in the self-assembly of amyloid fibrils. *FASEB J* 2002;16:77–83.
66. Sacchettini JC, Kelly JW. Therapeutic strategies for human amyloid diseases. *Nat Rev Drug Discov* 2002;1:267–275.
67. Dobson CM. Protein folding and misfolding. *Nature* 2003;426:884–890.
68. Petkova AT, Leapman RD, Guo Z, Yau WM, Mattson MP, Tycko R. Self-propagating, molecular-level polymorphism in Alzheimer's β -amyloid fibrils. *Science* 2005;307:262–265.
69. Krishnan R, Lindquist SL. Structural insights into a yeast prion illuminate nucleation and strain diversity. *Nature* 2005;435:765–772.

Copyright of Amyloid is the property of Taylor & Francis Ltd and its content may not be copied or emailed to multiple sites or posted to a listserv without the copyright holder's express written permission. However, users may print, download, or email articles for individual use.